RSC Advances

ROYAL SOCIETY OF CHEMISTRY

www.rsc.org/advances

Size-and Phase-Dependent Structure of Copper (II) Oxide Nanoparticles

Alauddin Ahmed, Paolo Elvati, and Angela Violi*

Department of Mechanical Engineering, Chemical Engineering,
University of Michigan
Ann Arbor, Michigan 48109-2125, United States
Phone: 734-615-6448; Fax: 734-647-9379

(*All Correspondence should be made to: avioli@umich.edu)

Abstract

Copper (II) oxide (CuO) nanoparticles (NPs) have found numerous applications in electronics, optics, catalysis, energy storage, health, and water purification. Controlled synthesis of CuO NPs requires information on their nanoscale structure, which is expected to vary depending on the size, shape, phase, and most importantly, on the surface morphology. In this work, we report a detailed analysis of the structure of solid and melted CuO nanoparticles as functions of size and temperature at global and local scales, using molecular dynamics simulations. Comparisons of simulated X-ray diffraction profiles, mean bond lengths, average coordination numbers, and melting points with available experimental data support the modeling results. Melting points of CuO NPs vary linearly with the reciprocal of the diameters of NPs. The long-range order seen in solid nanoparticles with diameters greater than 6nm gradually vanishes as size decreases, indicating the loss of translational symmetry of the lattice structure and the emergence of amorphous-like structure even below the melting point. Melted nanoparticles show liquid-like characteristics with only a short-range order. Mean bond lengths and average Cu-O coordination numbers of both solid and melted NPs indicate weakening of the structural stabilization for smaller NPs that leads to an increased deformation in the local atomic arrangement because of the lack of long-range interactions. For the cases studied, most of the structural features are independent of temperature, with the notable exception of the number of oxygen atoms coordinated to Cu. This latter quantity is indeed indicative of melting phase transition and can be used to compute the melting point accurately. Atoms on the surface of solid NPs show amorphous-like behavior even at temperatures well below the melting point of the NPs due to the limited coordination environment. This study represents a useful step towards the establishment of a structure-property relationship for CuO nanoparticles.

KEYWORDS: Copper oxide, structure, melting point, surface, and molecular dynamics.

Introduction

Many of the fascinating features of nanoparticles (NPs) are due to their large surface volume ratio, structure and morphology that dictate surface-mediated reactions, nucleation, and growth mechanisms.[1–4] Copper (II) oxide NPs have found a multitude of applications[5–10] in the fields of catalysis,[11, 12] semiconducting and superconducting materials, lubricants, electronics, optics,

sensors,[13] spintronics, and health.[14] Examples of cutting-edge utilizations of CuO NPs include arsenic removal from water,[15] fabrication of lithium ion battery,[16] rocket propellant combustion, and antimicrobial.[17] Despite the remarkable technological importance of this material, the literature on atomic scale investigations of CuO NPs is very limited as compared with other metal oxide nanoparticles, such as TiO_2,[18–20] Al_2O_3,[21] SiO_2,[22, 23] CeO_2, and ZnO.

Recently, Rodrigo[24] has observed different XANES (X-ray absorption near edge structure) spectra between solid and bulk phases of CuO, and he attributed this feature to the different coordination geometry of Cu atoms during the synthesis process. Zhang et al. have highlighted the importance of surface characteristics, consisting of under-coordinated[25] atoms of dissimilar ionic radii and dangling bonds, in catalysis and surface mediated reactions for CuO NPs.[13]

The nature of the atomic interactions at the nanoscale,[26, 27] however, depends on the environment and thermophysical conditions.[28] This information is hard to obtain experimentally, not only because of the length and timescales involved, but mostly because the synthesis of monodisperse nanoparticles is difficult to realize and hence the structure, thermodynamics, and dynamics measures become complicated by polydispersity, impurities, and defects.

Atomistic simulations represent a powerful tool that can provide insights on the molecular mechanisms that drive and control the interactions at the nanoscale. Furthermore, atomic scale data of NPs via molecular simulations are also important for understanding and interpreting the experimental information obtained from X-ray diffraction (XRD), neutron scattering, EXFAS (extended X-ray absorption fine structure spectroscopy), XANES, WAXS (wide-angle X-ray scattering), XAS (X-ray absorption spectroscopy).[1, 18, 19, 29] For these reasons, a considerable effort has been devoted to understand the structures of solid, amorphous, and liquid nanoparticles, including a few metal oxides,[18, 19, 30] using molecular simulation techniques.[18, 19, 22, 23, 31, 32] For CuO, however, there is still a limited understanding of its growth mechanisms as well as its physicochemical properties as a function of size, shape, and temperature.

In this paper, we report a comprehensive analysis of the atomic scale properties of solid and melted CuO NPs and their dependence on size and temperature using molecular dynamics simulation techniques. We examine structural properties using simulated XRD profiles, mean bond length, and coordination numbers.

Methodology

Force Field

Although, a number of force fields (FFs) are available for pure metals or for specific metal oxides (e.g., TiO_2, Al_2O_3,), the number of FFs for CuO is limited. On one side the use of fixed charge ionic potentials has shortcomings, as indicated by Zhou et al.[33] and Stolbov and Rahman,[34] on the other hand, the application of first principles methods to simulate nanoparticles is prohibitively expensive in terms of computational resources due to the number of atoms involved. A new version of the ReaxFF variable charge force field,[35] optimized for CuO and applicable to a wide range of temperatures,[36–38] was employed in this study. This force field was evaluated previously for bulk CuO by computing heat of formation and comparing it with DFT

prediction which were -43.2 kcal/mol and -37.3 kcal/mol, respectively.[36, 39, 40] Our choice was also motivated by the ability of ReaxFF to perform dynamic charge equilibrations dependent on local geometries at each time step.

ReaxFF force field computes the energy of a system considering the following partial contributions:

$$E_{system} = E_{bond} + E_{lp} + E_{over} + E_{under} + E_{val} + E_{pen} + E_{3conj} + E_{tors} + E_{4conj} + E_{H-bond} + E_{vdWaals} + E_{Coulomb} \quad (1)$$

where from first to the last symbolic terms represent energies due to bond, lone pair, over-coordination, under-coordination, valence angle (3-body), torsion angle (4-body), penalty, 3-body conjugated, 4-body conjugation, hydrogen bond interactions, van der Waals interactions, and Coulomb interactions, respectively. Details of each energy contributions including complete functional forms can be found in the work by van Duin et al.[41, 42] In contrast to fixed charge force fields, ReaxFF uses variable charges computed on the fly using electron equilibrium method[43] and considering charge transfer and polarization. Also, instead of fixed connectivity between atoms, ReaxFF computes bond order from instantaneous interatomic distances, which allows bond breaking and formation. The pairwise van der Waals interactions and electrostatic interactions are modeled using distance corrected (to limit excessive repulsive interactions between bonded atoms and atoms shearing a valence angle) Morse-potential and Coulomb potential, respectively. ReaxFF also applies a Taper correction (7th order polynomial function) to avoid energy discontinuities when charged species move in and out of the non-bonded cutoff radius. The parameters for CuO relevant to the energy terms in eqn. (1) can be found in the Supplementary Information of the literature by van Duin.[36]

Simulation Details

Molecular dynamics simulations were carried out for four spherical CuO nanoparticles with diameters of 2nm, 3nm, 4nm, and 6nm consisting of 416, 1404, 3362, and 11326 atoms, respectively. The initial configurations were obtained via a spherical cut of a super lattice generated from monoclinic CuO lattice parameters, using Accelrys Materials Studio software. To maintain charge balance, excess ions were removed from the surface. All the nanoparticles considered were spherical, as reported from different synthesis routes,[44] as well as by the size range chosen for our work.

Molecular dynamics simulations were carried out in vacuum using the LAMMPS package.[45]The simulations were run at constant temperature employing the Berendsen thermostat [46, 47] without periodic boundary conditions and with an integration step of 0.01 fs. All the systems were equilibrated for up to 250 ps depending on the system size, temperature and the analysis performed.

X-ray diffraction (XRD) profiles at a wavelength of 1.5418 Å were computed using Debye scattering formula:[48–50]

$$I(Q) = \sum_i \sum_j f_i f_j \frac{\sin(Q r_{ij})}{Q r_{ij}}$$

Where $I(Q)$is the scattering intensity, $r_{ij} = |r_i - r_j|$is the distance between atoms i and j and Q is the atomic scattering vector which is a momentum transfer vector defined by

$$Q = |\vec{Q}| = \frac{4\pi sin\theta}{\lambda}$$

where θ is the diffraction half-angle and λ is the radiation wavelength.

Results and Discussion

The effect of structural properties on melting point is an important information and as first step we investigated the size dependence of the melting points. Empirical models[51–53] for different metal oxides can be found in the literature, but none of them is specific for for CuO. To determine the melting points of NPs of various sizes, we carried out simulations at intervals of 100K. We monitored the potential energy profile, isochoric heat capacity, and radial distribution function to locate the melting point. Figure 1 shows the computed potential energy profile, isochoric heat capacities, and radial distribution functions at melting point (1100 ± 50 K) for a 4 nm CuO NP.

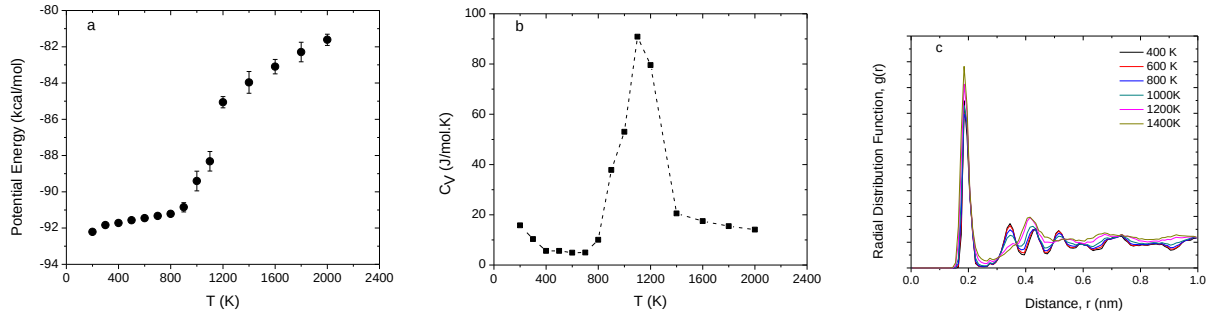

Figure 1 Computed (a) potential energy profile, (b) isochoric heat capacity profile, and (c) radial distributions as functions of temperature for a 4 nm CuO NP.

Figure 2 shows the comparison between our MD simulations (filled circles) and the values obtained from the empirical model proposed by Jiang-Shi.[53] The latter bases its prediction on the bulk properties of the materials and has been used for other metal oxides.[54, 55] We extended the empirical model to include the physical properties of CuO; further details can be found in the Supplementary Information (SI).

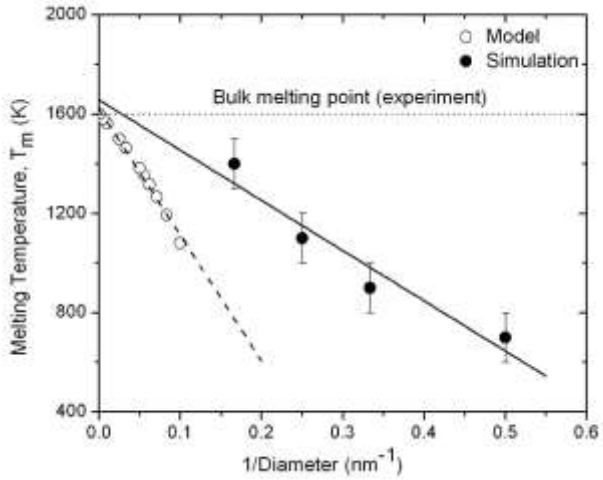

Figure 2 Melting temperatures of spherical CuO NPs as a function of the inverse of diameters computed with MD (solid circles) and predicted by Jiang-Shi's model. Solid and dashed lines show the linear fits of the results. The bulk melting temperature as determined with MD is 1657±132 K. Dotted line shows the melting temperature for the bulk (1600 K) as determined experimentally.[56]

Molecular dynamics results show the expected decrease in melting temperatures as the diameter of the NP increases, a phenomenon commonly observed for other nanomaterials, including metals and metal oxides.[51–53, 57] An important point is the ability of MD simulations to reproduce the experimental value of the bulk melting point: despite the limited number of simulated NPs, the extrapolation of the bulk melting point (1657 ± 132 K) is in agreement with the experimental value of 1600 K.[56]

While both the MD simulations and the empirical model predict the same trend, the difference between them increases rapidly as the diameters of NPs are reduced. Without an experimental measure of the melting point of the nanoparticles is hard to conclude the relative quality of these two methods. However, the MD method shows consistency and applicability to a broad range of sizes. It can predict the bulk melting point using information on the computed melting temperatures of nanoparticles. In addition, the empirical model is applicable only to nanoparticles as small as 4 nm.[53, 58, 59]

Based on these results, we simulated solid NPs at 300 K and melted NPs at 1700 K. To examine their structures, we computed their XRD profiles and compared with the experimental XRD patterns of bulk CuO. Figure 3 shows the simulated XRD profiles and the experimental pattern

(ICSD: 67850).[60, 61] XRD data clearly differentiates between the two states (solid and melted), except for very small NPs (2 nm in diameter). Peaks in the XRD plots of solid NPs (Figure 3a) indicate the presence of a CuO monoclinic phase. The match between the XRD profiles of the solid NPs and the bulk increases with the diameters of NPs, transitioning from the amorphous-like spectrum of the smallest (2 nm) NP to the biggest NP (6 nm). NP melts are characterized by a disordered structure (so called "x-ray amorphous"[18]) that results in flattened characteristic peaks as reported in Figure 3b.

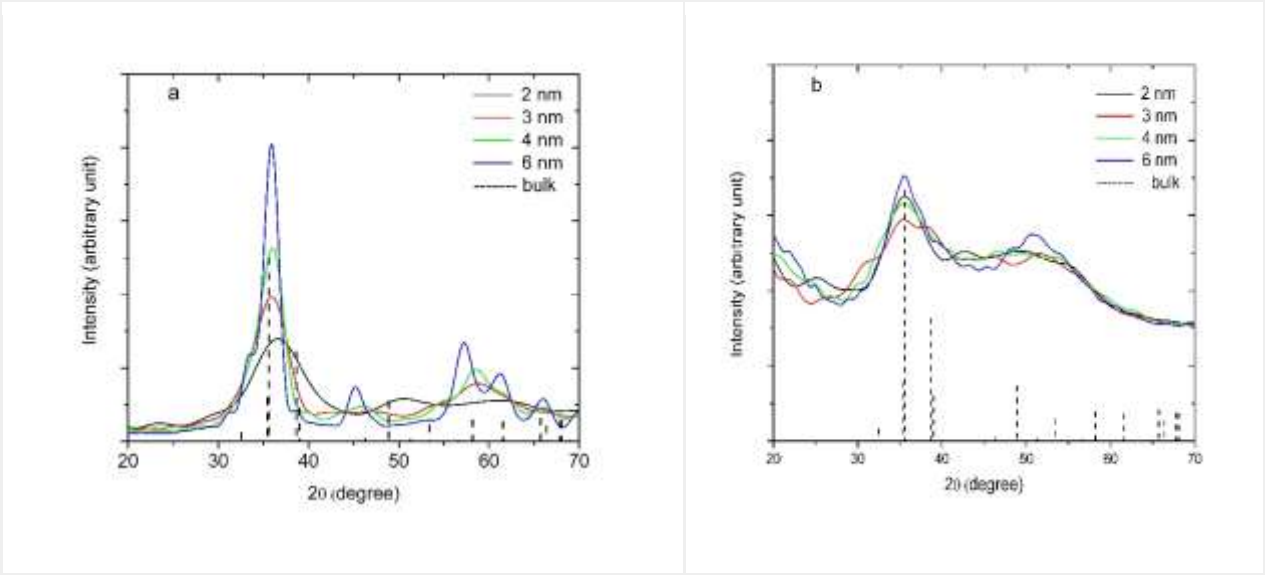

Figure 3 Simulated X-ray diffraction (XRD) profiles for (a) solid (300 K) and (b) melted (1700 K) CuO nanoparticles of different diameters. The positions of the peaks of the experimental[60, 61] XRD profile of bulk CuO are shown as dashed vertical lines.

While XRD diffraction profiles describe the global structure, the average Cu-O and Cu-Cu first nearest neighbor distances can provide information on the short range atom arrangement. These values are computed as the first moment of the distribution of the Cu-O and Cu-Cu minimum distances.

For solid NPs, the Cu-O bond length slightly decreases with the size of NPs (Figure 4a). Linear fit of the mean bond lengths as a function of the reciprocal diameters predicts bulk Cu-O bond length of 0.194 nm that is in great agreement with the experimental value of 0.1954 ± 0.0005 nm,[62, 63] obtained from XRD at low temperature and the value of 0.1944 ± 0.0010 nm[63] measured with EXAFS for the bulk crystal. This value is higher than the theoretical value of 0.181 nm[64] obtained from density functional theory calculation using B3LYP/LANL2DZ and experimental value of 0.1704 nm[65] obtained for a single CuO molecule at 0K. This discrepancy is unsurprising as single molecules are expected to have a different bond length than NPs or bulk systems. Similar size-dependent bond lengths of solid NPs were reported earlier[66] for metal and metal oxide NPs.

Differently from solid NPs, the mean bond lengths of melted NPs (Figure 4b) are slightly shorter and marginally vary with the system size between 0.191 ± 0.004 nm (2 nm NP) and 0.193 ± 0.004 (6 nm NP). A similar shortening of metal-oxygen bond length has been previously

reported for amorphous TiO_2 nanoparticles compared to bulk anatase,[18] once again confirming the amorphous nature of CuO NP melts.

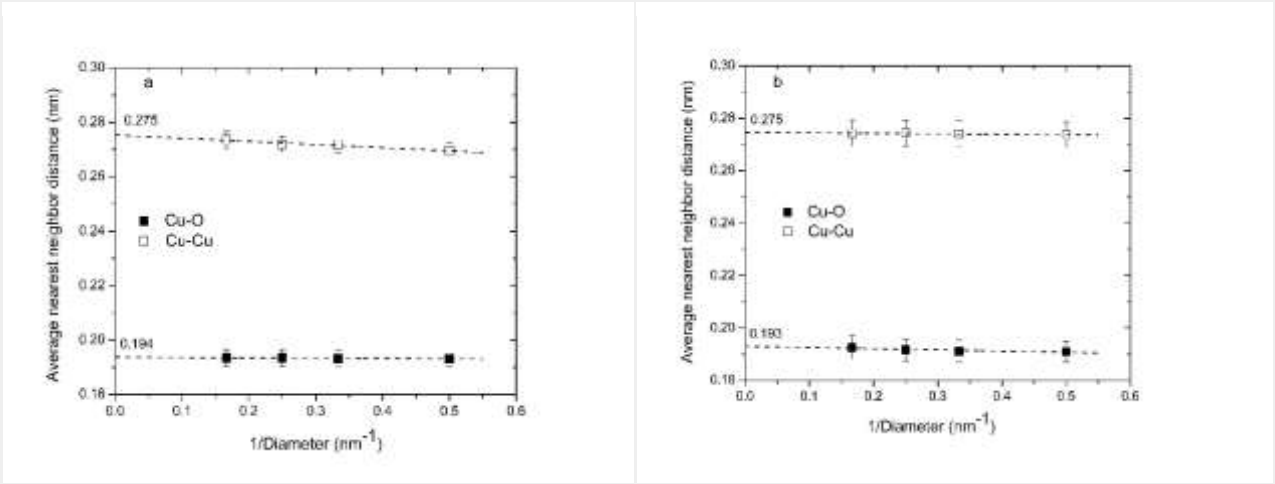

Figure 4 Mean Cu-O and Cu-Cu first neighbor distances of (a) solid (300 K) and (b) melted (1700 K) CuO NPs as a function of the inverse diameter. Dashed lines show the linear fits.

The results for the Cu-Cu nearest neighbor distances indicate opposite phase trends. Solid phase Cu-Cu nearest neighbor distances are more sensitive to the size of the system than to those of the melted phase, even though the predicted bulk values are the same (0.275 nm). In fact, the Cu-Cu nearest neighbor distances for melted NPs is all within their standard errors. In contrast, for solid NPs Cu-Cu nearest neighbor distances vary between 0.270 ± 0.003 nm (for 2nm NP) and 0.274 ± 0.003 nm (for 6 nm NP).

To augment the information on local structure given by the average first neighbor distances, we analyzed the local environment of the atoms by computing the average number of oxygen coordinated to Cu in the melt and solid states. The coordination number (CN) was obtained by computing the ensemble average of the RDF integral up to the minimum after the first peak. The computed coordination numbers as a function of the inverse of NP diameter (Figure 5) show that the CNs are smaller in the melt than the solid state, as expected due to the change in entropy associated with melting. For both solid and melted NPs, however, the CN has strong size dependence, increasing with decreasing NP size. Extrapolated CNs of solid NPs are in reasonable agreement with the standard bulk value of 4 for the Cu-O coordination. [63, 67] Cu-O coordination of a solid nanoparticle with a diameter of 2 nm is mostly pentahedral (CN=5) instead of tetrahedral. This increased CN is a consequence of the reduced stabilization of surface atoms from long range interactions compensated by an increase of short-range interactions. This increased "effective surface pressure"[18] is reflected in the deformation of monoclinic crystallographic planes observed in smaller CuO NPs. The same effect is visible in the melted NPs, even though in this case the extrapolated bulk CN value is 3.7. Similar reduction in CN of oxide melts (Y_2O_3, Ho_2O_3, La_2O_3, ZrO_2, and Al_2O_3) has been very recently reported using both experiments (combining aerodynamic levitation, neutron and X-ray diffraction) and MD simulations.[68–70]

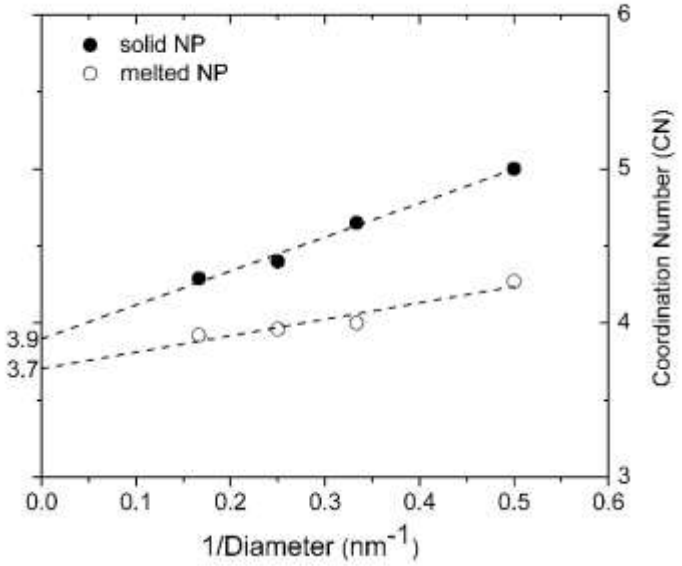

Figure 5 Coordination numbers as a function of the inverse of diameters of nanoparticles. Dashed lines show the linear fit of the data.

The understanding of the phase transition mechanism in CuO NPs requires a different approach, as it involves exploring a first order phase transition (see Figure 1). However, information can be inferred by looking at the thermal dependence of structural data. Therefore, we studied a CuO NP with a diameter of 4 nm in two temperature intervals: 300-600K for the solid state and 1500-1800K for the melted phase (Figure S2 in the SI). We chose a size of 4 nm, since it is the smallest size for which we can still observe a clearly distinct behavior between solid and melted phases.

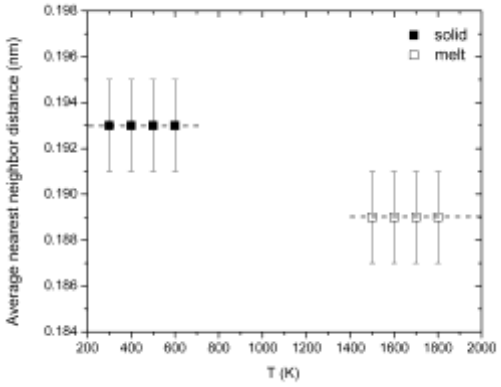

Figure 5 Mean Cu-O bond lengths as a function of temperature in the solid and melted phases.

Figure 5 shows the mean Cu-O bond lengths at different temperatures in both solid and melted NPs. Unsurprisingly, the bonding distance depends on the phase with a slight contraction observed in the melted NP. Similar contraction of bond distances has been recently reported for the melted Cu and for other pure metal nanoparticles using both experiments (XRD and/or

EXAFS) and molecular dynamics techniques.[71, 72] Moreover, a similar behavior was previously found for the melts of other pure metals[72–74] and alloys.[75, 76] Both in the solid and melted phases Cu-O bond distances are independent of temperature, in agreement with previous results for CuO NPs and bulk, obtained respectively, from XRD and EXAFS[63] measurements. The temperature dependence of the CN of oxygen atoms around Cu atoms (Figure 6) is striking.

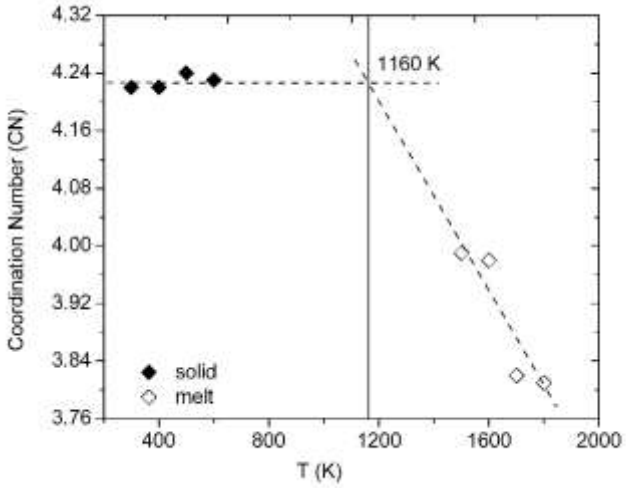

Figure 6 Temperature dependence of the numbers of oxygen atoms coordinated around Cu in a 4 nm (diameter) CuO NP.

In both phases the CN decreases with increasing temperature, and while the effect is almost negligible in the solid phase, it is very pronounced for the melted NPs. This result is in agreement with the CNs' trends shown above and a consequence of the balance between enthalpic and entropic contributions. Interestingly, the temperature dependence is linear within the limit of the error and therefore CN can be used to estimate the melting temperature. For example for the 4 nm NP, extrapolation of the CN predicts a melting temperature of 1160 ± 50K in great agreement with the 1100 ± 50 K value obtained from Figure 1.

Due to the high surface to volume ratio typical of NPs, many properties are potentially affected by surface behavior, which is normally negligible in bulk. Therefore, we decided to investigate to which extent outer and inner layers of the CuO NPs differ. Since for small NPs it is hard to distinguish between surface and core atoms, we studied NPs with a diameter of 4 nm. Our previous results show that this is the smallest size where "bulk" behavior begins to appear and therefore we expect this NP to show the strongest surface effects. We defined the surface as the NP's outermost layer having a thickness of 0.36 nm (approximately twice Cu-O bond length), as a compromise between statistical error (from the small number of atoms) and error due to averaging of the surface and core properties.

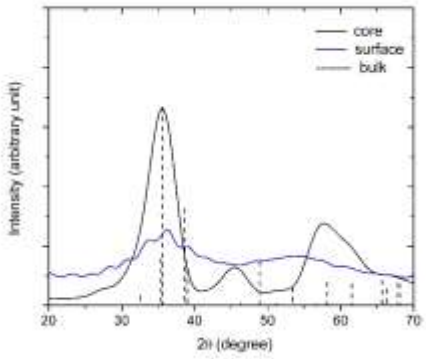

Figure 7 Simulated X-ray diffraction (XRD) profiles of the surface (blue) and core (black) of a CuO NP of 4 nm in diameter at 300 K. The positions of the peaks of the experimental XRD profile of bulk CuO are shown as dashed vertical lines.

A comparison of the core and surface XRD profiles for solid NP (see Figure 7) suggests that surface structure does not have the monoclinic features present in the core structure as shown in Figure 8.

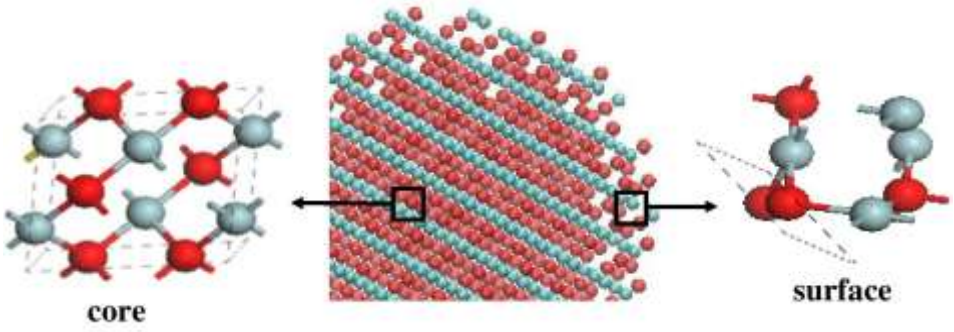

Figure 8 Structures of core and surface of CuO NP. Red and blue represent oxygen and copper (II) ions, respectively.

The XRD profile shows an amorphous-like organization for the surface of a solid 4 nm NP even at room temperature, far below the melting point. This effect is probably caused by the truncation of crystal plane at the surface due to the high curvature of the NP. Similar distorted surface was previously observed experimentally for nearly spherical CuO nanoparticles using transmission electron microscopy (TEM).[13] Based on these results, we expected the surface and core of a melted NP to produce similar XRD profile.

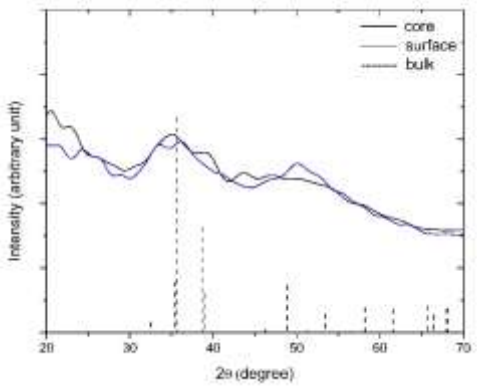

Figure 9 Simulated X-ray diffraction (XRD) profiles of the surface (blue) and core (black) of a CuO NP of 4 nm in diameter at 1700 K. The positions of the peaks of the experimental XRD profile of bulk CuO are shown as dashed vertical lines.

While this is generally true, as shown in Figure 9, there are slight differences. In both cases here is no indication of long-range order in either the core or the surface plot, which confirms the amorphous structure. However, the XRD plot of the core shows a characteristic[18] broad and weak hump at 35° whereas the surface profile is flattened, although slightly noisy. This difference suggests amorphous structures of different stoichiometry for the surface and core.

Conclusions

In this paper, we reported a detailed analysis of the nanoscale structure of CuO nanoparticles using molecular dynamics simulations, and compared the results with available experimental data. We investigated the properties of different phases as function of size and temperatures. As for other inorganic NPs, we found that the melting temperature is inversely proportional to the particle diameter, with a linear fit that predicted the experimental bulk melting temperature very well (1657K versus 1600K), and it estimated NP melting point better than generic empirical models. The comparison between predicted and experimental XRD profiles showed a remarkable agreement indicating monoclinic crystal structure for solid particles, as small as for particles of 4 nm in diameter. Global structural information was integrated with data on local geometries, such as first neighbors mean distance and Cu average coordination number. The results suggest distinct nanoscale structural features for the solid and melted NPs. Differently, particles with diameters of 2 nm do not show any clear core-surface or phase dependent distinction. These simulations results were confirmed by experimental observations of amorphous-like structures for NPs of 2 nm or less in diameter. Like other transition metal oxides, the Cu-O bond length in NPs is smaller than that of the bulk, with negligible temperature dependence, again in accordance with experimental data.

For nanoparticles with diameters of 4 nm, we observed key differences in properties depending on spatial position (surface vs core) and thermodynamic phase (melt vs solid). The local geometry of CuO NPs at different temperatures is modified not by virtue of bond change, which is only minimally dependent on NP size and phase, but by the atomic arrangement (quantified as coordination number, or CN). Since the phase dependence of the CNs is significant, CN can be

used as an indicator of the phase transformation. Atoms on the surface of a solid NP form an amorphous-like layer (or distorted outer shell) at temperatures well below the melting point. This phenomenon explains the existence of a rough spherical surface of CuO nanoparticles observed in TEM images. Notably, even the surface of melted NPs displays differences, from the core.

This study is a useful step towards the establishment of a structure-property relationship for CuO nanoparticles that is important for the understanding of nucleation, melting/freezing transition, sintering, aggregation, nanocomposite, and the growth of nanoparticles on other nanostructures (e.g., multi-walled carbon nanotube, nanoelectrode devices). These results will provide guidance for understanding the phase diagrams of mixed metal oxides and surface mediated reaction mechanisms in catalysis.

Supporting Information

Potential energy profiles versus time to demonstrate convergence; details about the empirical model to determine melting point; and temperature dependence of X-ray diffraction (XRD) profiles are given in the Supplementary Information.

Acknowledgements

This research has been funded by NSF through DMR1105361. This research was supported in part through computational resources and services provided by Advanced Research Computing at the University of Michigan, Ann Arbor.

References

[1] L.X. Chen, T. Rajh, Z. Wang, and M.C. Thurnauer, "XAFS Studies of Surface Structures of TiO2 Nanoparticles and Photocatalytic Reduction of Metal Ions," *J Phys Chem*, **101** 10688–10697 (1997).

[2] N. Wang, Y.H. Tang, Y.F. Zhang, C.S. Lee, I. Bello, and S.T. Lee, "Si nanowires grown from silicon oxide," *Chem. Phys. Lett.*, **299** [2] 237–242 (1999).

[3] N. Wang, Y. Caia, and R.Q. Zhang, "Growth of nanowires," *Mater. Sci. Eng. R Reports*, **60** [1-6] 1–51 (2008).

[4] G.C. Schatz, "Using theory and computation to model nanoscale properties," *PNAS*, **104** [17] 6885–6892 (2007).

[5] J.T. Lue, *Physical Properties of Nanomaterials, Volume X, Encycl. Nanosci. Nanotechnol.*, 1–46 (2004).

[6] A. Umar, M. Vaseem, and Y. Hahn, *Growth , Properties , and Applications of Copper Oxide and Nickel Oxide / Hydroxide Nanostructures*. 2010.

[7] T. Maruyama, "Copper oxide thin films prepared by chemical vapor deposition from copper dipivaloylmethanate," *Sol. Energy Mater. Sol. Cells*, **56** [1] 85–92 (1998).

[8] Y.P. Sukhorukov, N.N. Loshkareva, A.A. Samokhvalov, S. V Naumov, A.S. Moskvin, and A.S. Ovchinnikov, "Magnetic phase transitions in optical spectrum of magnetic semiconductor CuO," *J. Magn. Magn. Mater.*, **183** [3] 356–358 (1998).

[9] M. Frietsch, F. Zudock, J. Goschnick, and M. Bruns, "CuO catalytic membrane as selectivity trimmer for metal oxide gas sensors," *Sens Actuators B Chem*, **65** [1-3] 379–381 (2000).

[10] C.L. Carnes and K.J. Klabunde, "The catalytic methanol synthesis over nanoparticle metal oxide catalysts," *J. Mol. Catal. Chem.*, **194** [1-2] 227–236 (2003).

[11] S. Lee, *Methanol Synthesis Technology*. CRC Press, 1990.

[12] B.S. Anandakumar, M.B.M. Reddy, C.N. Tharamani, M.A. Pasha, and G.T. Chandrappa, "Combustion-derived CuO nanoparticles: An effective and environmentally benign catalyst in the synthesis of aromatic nitriles from aromatic aldehydes," *Chin. J. Catal.*, **34** [4] 704–710 (2013).

[13] J. Zhang, J. Liu, Q. Peng, and X. Wang, "Nearly Monodisperse Cu2O and CuO Nanospheres: Preparation and Applications for Sensitive Gas Sensors," *Chem Mater*, **18** 867–871 (2006).

[14] D. Gao, J. Zhang, J. Zhu, J. Qi, Z. Zhang, W. Sui, H. Shi, and D. Xue, "Vacancy-Mediated Magnetism in Pure Copper Oxide Nanoparticles," *Nanoscale Res Lett*, **5** [4] 769–772 (2010).

[15] K.J. Reddy, K.J. McDonald, and H. King, "A novel arsenic removal process for water using cupric oxide nanoparticles.," *J. Colloid Interface Sci.*, **397** 96–102 (2013).

[16] P. Poizot, S. Laruelle, S. Grugeon, L. Dupont, and J.M. Tarascon, "Nano-sized transition-metal oxides as negative-electrode materials for lithium-ion batteries.," *Nature*, **407** [6803] 496–9 (2000).

[17] A. Azam, A.S. Ahmed, M. Oves, M.S. Khan, and A. Memic, "Size-dependent antimicrobial properties of CuO nanoparticles against Gram-positive and-negative bacterial strains.," *Int. J. Nanomedicine*, **7** 3527–35 (2012).

[18] H. Zhang, B. Chen, J. Banfield, and G. Waychunas, "Atomic structure of nanometer-sized amorphous TiO2," *Phys. Rev. B*, **78** [21] 214106 (2008).

[19] P.K. Naicker, P.T. Cummings, H. Zhang, and J.F. Banfield, "Characterization of titanium dioxide nanoparticles using molecular dynamics simulations.," *J. Phys. Chem. B*, **109** [32] 15243–9 (2005).

[20] B. Buesser, a J. Gröhn, and S.E. Pratsinis, "Sintering Rate and Mechanism of TiO2 Nanoparticles by Molecular Dynamics.," *J Phys Chem C*, **115** [22] 11030–11035 (2011).

[21] Y. Li, R.K. Kalia, A. Nakano, and P. Vashishta, "Size effect on the oxidation of aluminum nanoparticle: Multimillion-atom reactive molecular dynamics simulations," *J. Appl. Phys.*, **114** [13] 134312 (2013).

[22] I. V Schweigert, K.E.J. Lehtinen, M.J. Carrier, and M.R. Zachariah, "Structure and properties of silica nanoclusters at high temperatures," *Phys Rev B*, **65** [23] 235410 (2002).

[23] M.R. Zachariah and M.J. Carrier, "Properties of Silicon Nanoparticles: A Molecular Dynamics Study," *J Phys Chem*, **100** [36] 14856–14864 (1996).

[24] U.I. Rodrigo, "Geometrical and Electronic Structure of Metal Oxide Nanoparticles on Silica and Alumina"; Ph.D. Thesis, Lousiana State University, 2012.

[25] C.Q. Sun, "Size dependence of nanostructures: Impact of bond order deficiency," *Prog. Solid State Chem.*, **35** 1–159 (2007).

[26] A. Barnard, C.M. Li, R. Zhou, and Y. Zhao, "Modelling of the nanoscale," *Nanoscale*, **4** [4] 1042 (2012).

[27] D. Spagnoli and J.D. Gale, "Atomistic theory and simulation of the morphology and structure of ionic nanoparticles.," *Nanoscale*, **4** [4] 1051–67 (2012).

[28] Y. Waseda and J.M. Toguri, *The Structure and Properties of Oxide Melts: Application of Basic Science to Metallurgical Processing*. World Scientific, Singapore, 1998.

[29] A.I. Frenkel, A. Yevick, C. Cooper, and R. Vasic, "Modeling the Structure and Composition of Nanoparticles by Extended X-Ray Absorption Fine-Structure Spectroscopy," *Ann Rev Anal Chem*, **4** 23–39 (2011).

[30] H. Zhang and J.F. Banfield, "Understanding Polymorphic Phase Transformation Behavior during Growth of Nanocrystalline Aggregates : Insights from TiO2," *J Phys Chem B*, **104** 3481–3487 (2000).

[31] H. Zhang and J.F. Banfield, "Phase transformation of nanocrystalline anatase-to-rutile via combined interface and surface nucleation," *J Mater Res*, **15** [2] 437–448 (2000).

[32] G. Jian, N.W. Piekiel, and M.R. Zachariah, "Time-Resolved Mass Spectrometry of Nano-Al and Nano-Al/CuO Thermite under Rapid Heating: A Mechanistic Study," *J Phys Chem C*, **116** 26881–26887 (2012).

[33] X.W. Zhou, H.N.G. Wadley, J. Filhol, and M.N. Neurock, "Modified Charge Transfer–Embedded Atom Method Potential for Metal/Metal Oxide Systems," *Phys Rev B*, **69** 035402 (2004).

[34] S. Stolbov and T.S. Rahman, "Relationship between Electronic and Geometric Structures of the O/Cu(001) System," *J Chem Phys*, **117** [18] 8523–8530 (2002).

[35] T. Liang, T. Shan, Y. Cheng, B.D. Devine, M. Noordhoek, Y. Li, Z. Lu, S.R. Phillpot, *et al.*, "Classical atomistic simulations of surfaces and heterogeneous interfaces with the charge-optimized many body (COMB) potentials," *Mater. Sci. Eng. R*, **74** [9] 255–279 (2013).

[36] A.C.T. Van Duin, V.S. Bryantsev, M.S. Diallo, W.A. Goddard, O. Rahaman, D.J. Doren, D. Raymand, and K. Hermansson, "Development and Validation of a ReaxFF Reactive Force Field for Cu Cation/Water Interactions and Copper Metal/Metal Oxide/Metal Hydroxide Condensed Phases," *J Phys Chem*, **114** [35] 9507–9514 (2010).

[37] X. Duan, O. Warschkow, A. Soon, B. Delley, and C. Stampfl, "Density functional study of oxygen on Cu(100) and Cu(110) surfaces," *Phys. Rev. B*, **81** [7] 075430 (2010).

[38] B. Jeona, S.K.R.S. Sankaranarayanan, A.C.T. van Duin, and S. Ramanathan, "Influence of surface orientation and defects on early-stage oxidation and ultrathin oxide growth on pure copper," *Phil Mag*, **91** [32] 4073–4088 (2011).

[39] B. Jeon and S.K.R.S. Sankaranarayanan, "Influence of Surface Orientation and Defects on Early-Stage Oxidation and Ultrathin Oxide Growth on Pure Copper," *Philos. Mag.*, **91** [32] 4073–4088 (2011).

[40] B. Jeon, S.K.R.S. Sankaranarayanan, A.C.T. Van Duin, and S. Ramanathan, "Reactive Molecular Dynamics Study of Chloride Ion Interaction with Copper Oxide Surfaces in Aqueous Media," *Acs Appl Mater Interfaces*, **4** [3] 1225–1232 (2012).

[41] A.C.T. van Duin, S. Dasgupta, F. Lorant, and W. a. Goddard, "ReaxFF: A Reactive Force Field for Hydrocarbons," *J. Phys. Chem. A*, **105** [41] 9396–9409 (2001).

[42] A.C.T. Van Duin, A. Strachan, S. Stewman, Q. Zhang, X. Xu, and W.A. Goddard, "Reactive Force Field for Silicon and Silicon Oxide Systems," [1] 3803–3811 (2003).

[43] W.J. Mortier, S.K. Ghosh, and S. Shankar, "Electronegativity Equalization Method for the Calculation of Atomic Charges in Molecules," *J Am Chem Soc*, **108** 4315–4320 (1986).

[44] C.-Y. Chiang, K. Aroh, and S.H. Ehrman, "Copper oxide nanoparticle made by flame spray pyrolysis for photoelectrochemical water splitting – Part I. CuO nanoparticle preparation," *Int J Hydrog. Energy*, **37** [6] 4871–4879 (2012).

[45] S. Plimpton, "Fast Parallel Algorithms for Short–Range Molecular Dynamics," *J Comput Phys*, **117** 1–19 (1995).

[46] H.J.C. Berendsen, J.P.M. Postma, W.F. van Gunsteren, A. DiNola, and J.R. Haak, "Molecular dynamics with coupling to an external bath," *J. Chem. Phys.*, **81** [8] 3684 (1984).

[47] R.J. Sadus, *Molecular simulation of fluids: theory, algorithms, and object-orientation.* Elsevier, Amsterdam, 1999.

[48] P. Debye, "Zerstreuung von Rontgenstrahlen," *Ann Phys.*, **46** 809–823 (1915).

[49] C.L. Farrow and S.J.L. Billinge, "Relationship between the atomic pair distribution function and small-angle scattering: implications for modeling of nanoparticles research papers," *Acta Cryst*, **A65** 232–239 (2009).

[50] M. Wojdyr, *Debyer*. http://debyer.readthedocs.org/en/latest/, 2011.

[51] V.N. Koparde and P.T. Cummings, "Sintering of titanium dioxide nanoparticles: a comparison between molecular dynamics and phenomenological modeling," *J. Nanoparticle Res.*, **10** [7] 1169–1182 (2008).

[52] Y. Xing and D.E. Rosner, "Prediction of spherule size in gas phase nanoparticle synthesis," *J Nanopart Res*, **1** 277–291 (1999).

[53] Z. Zhang, X.X. Lu, and Q. Jiang, "Finite size e effect on melting enthalpy and melting entropy of nanocrystals," *Phys. B*, **270** 249–254 (1999).

[54] P.A. Bhatt, A. Pratap, and P.K. Jha, "Size And Dimension Dependent Diffusion Coefficients Of SnO2 Nanoparticles," *Aip Conf. Proc.*, **1536** 237–238 (2013).

[55] S. Mishra, S.K. Gupta, P.K. Jha, and A. Pratap, "Study of dimension dependent diffusion coefficient of titanium dioxide nanoparticles," *Mater. Chem. Phys.*, **123** [2-3] 791–794 (2010).

[56] *Material Safety Data Sheet: Copper (II) Oxide*. Iowa State University, 2003.

[57] P.A. Bhatt, A. Pratap, and P.K. Jha, "Study of size-dependent glass transition and Kauzmann temperatures of tin dioxide nanoparticles," *J Therm Anal Calorim*, **110** 535–538 (2012).

[58] X. Zheng, C. Xu, K. Nishikubo, K. Nishiyama, W. Higemoto, W. Moon, E. Tanaka, and E. Otabe, "Finite-size effect on Néel temperature in antiferromagnetic nanoparticles," *Phys. Rev. B*, **72** [1] 014464 (2005).

[59] X. Lang and Q. Jiang, "Size dependence of phase transition temperatures of ferromagnetic, ferroelectric and superconductive nanocrystals," *Front. Phys. China*, **2** [3] 289–311 (2007).

[60] G. Bergerhoff and I.D. Brown, "Crystallographic Databases"; in *Crystallogr. Databases*. International Union of Crystallography, 1987.

[61] A. Belsky, M. Hellenbrandt, V.L. Karen, and P. Luksch, "New developments in the Inorganic Crystal Structure Database (ICSD): accessibility in support of materials research and design research papers," *Acta Cryst*, **B58** 364–369 (2002).

[62] S. Asbrink and L.-J. Norrby, "A Refinement of the Crystal Structure of Copper (II) Oxide with a Discussion of Some Exceptional E.s .d.' s," *Acta Cryst*, **B26** [8] 8–15 (1970).

[63] L. Troger, T. Yokoyama, D. Arvanitis, T. Lederer, M. Tischer, and K. Baberschke, "Determination of bond lengths, atomic mean-square relative displacements, and local thermal expansion by means of soft-x-ray photoabsorption," *Phys Rev B*, **49** [2] 888–904 (1994).

[64] G. Bae, B. Dellinger, and R.W. Hall, "Density functional calculation of the structure and electronic properties of CunOn (n=1-8) clusters," *J Phys Chem*, **115** [11] 2087–2095 (2011).

[65] M.L. Polak, M.K. Gilles, J. Ho, and W.C. Lineberger, "Photoelectron Spectroscopy of CuO-," *J Phys Chem*, **95** 3460–3463 (1991).

[66] R. Vajtai, "Science and Engineering of Nanomaterials"; in *Springer Handb. Nanomater.* Edited by R. Vajtai. Springer, New York, 2013.

[67] M.S.P. Francisco, V.R. Mastelaro, A.O. Florentino, and D. Bazin, "Structural study of copper oxide supported on a ceria-modified titania catalyst system," *Top. Catal.*, **18** [January] 105–111 (2002).

[68] L.B. Skinner, C.J. Benmore, J.K.R. Weber, J. Du, J. Neuefeind, S.K. Tumber, and J.B. Parise, "Low Cation Coordination in Oxide Melts," *Phys Rev Lett*, **112** [15] 157801 (2014).

[69] L.B. Skinner, C.J. Benmore, J.K.R. Weber, S. Tumber, L. Lazareva, J. Neuefeind, L. Santodonato, J. Du, *et al.*, "Structure of Molten CaSiO3: Neutron Di ff raction Isotope Substitution with Aerodynamic Levitation and Molecular Dynamics Study," *J Phys Chem B*, **116** 13439–13447 (2012).

[70] L.B. Skinner, A.C. Barnes, P.S. Salmon, L. Hennet, H.E. Fischer, C.J. Benmore, S. Kohara, J.K.R. Weber, *et al.*, "Joint diffraction and modeling approach to the structure of liquid alumina," *Phys Rev B*, **87** 024201 (2013).

[71] H. Lou, X. Wang, Q. Cao, D. Zhang, J. Zhang, T. Hu, and H. Mao, "Negative expansions of interatomic distances in metallic melts," *PNAS*, **110** [25] 10068–10072 (2013).

[72] D. Holland-Moritz, T. Schenk, R. Bellissent, V. Simonet, K. Funakoshi, J.M. Merino, T. Buslaps, and S. Reutzel, "Short-range order in undercooled Co melts," *J Nano-Cryst. Solids*, **312-314** 47–51 (2002).

[73] T. Schenk, V. Simonet, R. Bellissent, and D.M. Herlach, "Icosahedral Short-Range Order in Deeply Undercooled Metallic Melts," *Phys Rev Lett*, **89** [7] 075507 (2002).

[74] T. Itami, S. Munejiri, T. Masaki, H. Aoki, Y. Ishii, T. Kamiyama, Y. Senda, F. Shimojo, *et al.*, "Structure of liquid Sn over a wide temperature range from neutron scattering experiments and first-principles molecular dynamics simulation: A comparison to liquid Pb," *Phys Rev B*, **67** [6] 064201 (2003).

[75] K. Georgarakis, D. V Louzguine-luzgin, and J. Antonowicz, "Variations in atomic structural features of a supercooled Pd–Ni–Cu–P glass forming liquid during in situ vitrification," *Acta Mater.*, **59** [2] 708–716 (2011).

[76] N.A. Mauro, W. Fu, J.C. Bendert, Y.Q. Cheng, E. Ma, and K.F. Kelton, "Local atomic structure in equilibrium and supercooled liquid Zr(75.5)Pd(24.5).," *J. Chem. Phys.*, **137** [4] 044501 (2012).

[77] J.L. Caslavsky and D.J. Viechnicki, "Melting behaviour and metastability of yttrium aluminium garnet (YAG) and YAIO3 determined by optical differential thermal analysis," *J Mater Sci*, **15** 1709–1718 (1980).

[78] W.H. Zachariasen, "The atomic arrangement in glass," *J Am Chem Soc*, **54** 3841–3851 (1932).

[79] C.B. Agee, "Crystal-liquid density inversions in terrestrial and lunar magmas," *Phys Earth Planet Inter*, **107** 63–74 (1998).

[80] D.R. Olander, *Fundamental aspects of nuclear reactor fuel elements: Solutions to problems*. U.S. Department of Energy, Washington, D.C., 1976.

[81] M. Zinigrad, L. Leontiev, E. Pastukhov, M. Shalimov, and S. Shanchurov, "Constitution and Model Description of the Structural Characteristics of Metallurgical Melts"; pp. 33–134 in *Phase Interact. Met.-Oxide Melts-Gas-Syst. Model. Struct. Prop. Process.* Springer, 2012.

[82] S. Sun, Y. Sun, X. Zhang, H. Zhang, X. Song, and Z. Yang, "A surfactant-free strategy for controllable growth of hierarchical copper oxide nanostructures," *CrystEngComm*, **15** 5275–5282 (2013).

[83] C. Karunakaran, G. Manikandan, and P. Gomathisankar, "Microwave, sonochemical and combustion synthesized CuO nanostructures and their electrical and bactericidal properties," *J. Alloys Compd.*, **580** 570–577 (2013).

[84] K.S. Ro, A. Venugopal, D.D. Adrian, D. Constant, K. Qaisi, K.T. Valsaraj, L.J. Thibodeaux, and D. Roy, "Solubility of 2, 4, 6-Trinitrotoluene (TNT) in Water," *J Chem Eng Data*, **41** [4] 758–761 (1996).

Figure for TOC

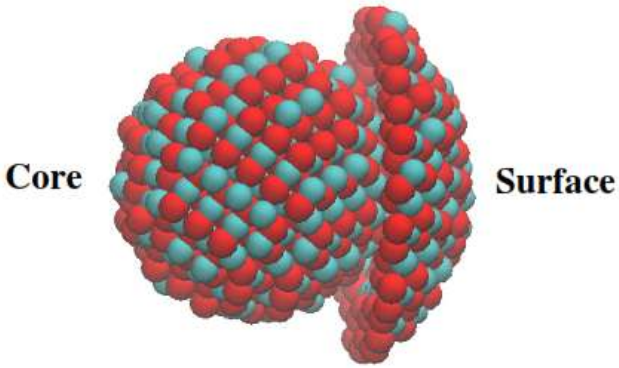

Figure Core (3 nm diameter) and outer surface layer (0.5 nm width) of a NP of 4 nm in diameter.